UiT
THE ARCTIC
UNIVERSITY
OF NORWAY

Faculty of Science and Technology
Department of Physics and Technology

Correction Strategies for Breathing Induced Motion in PET Images

Stian Bakkevoll

FYS-3941 Master's thesis in applied physics and mathematics June 2019

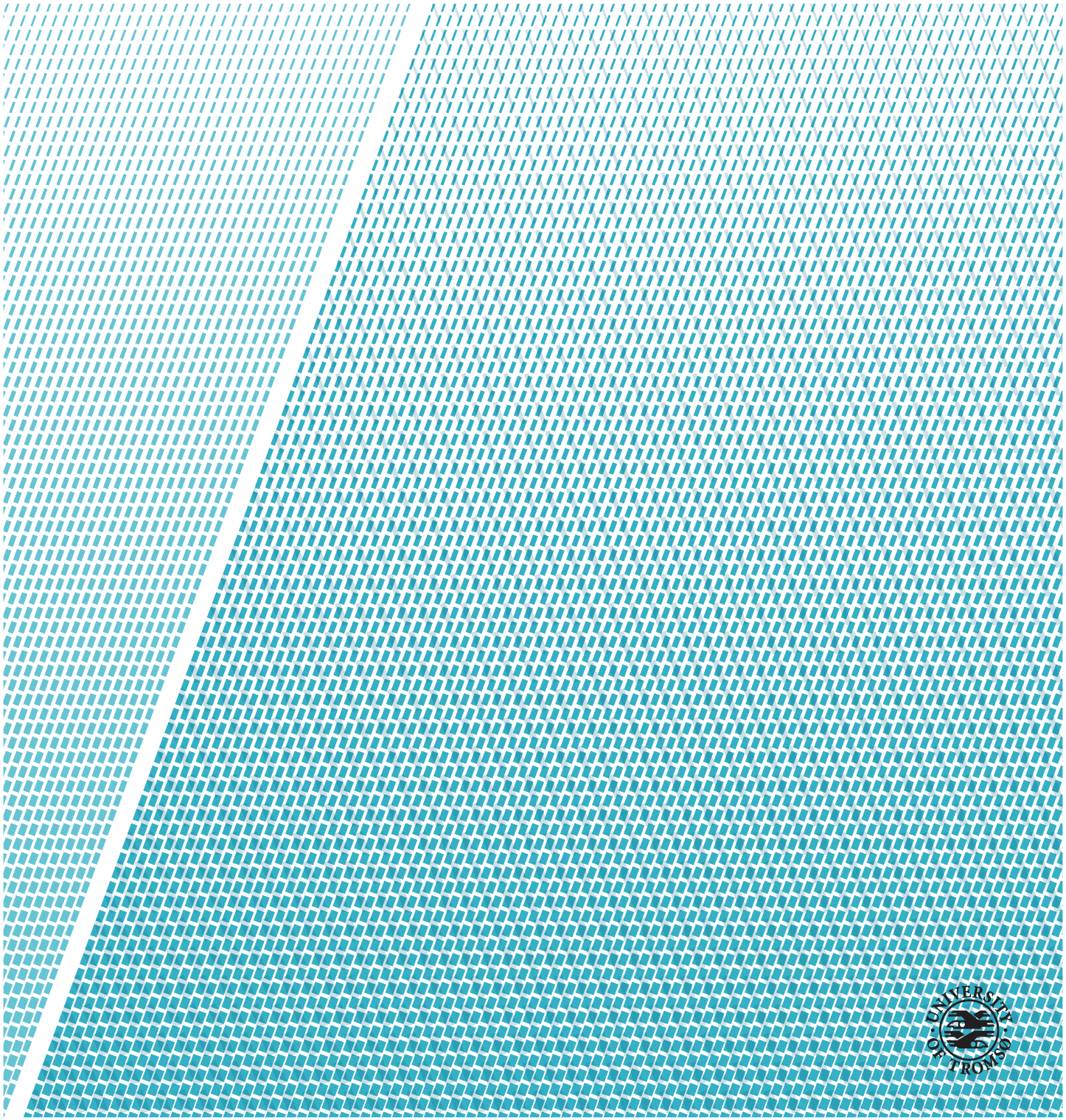

Abstract

Breathing induced motion highly impacts the quality of PET images. Motion blur impacts important parameters such as standardised uptake value (SUV) and lesion volume. To be able to stage lung cancer correctly, and provide correct treatment, the impact of motion needs to be reduced.

There exists techniques to combat the breathing motion, such as elastic motion correction and gating strategies. The aim of this thesis is to compare these three methods, and develop new methods involving dynamic frame reconstruction of PET images. The new strategies are not dependent on external equipments, and can be applied directly to attenuation corrected dynamic frames.

The results show that elastic motion correction is far better then most gating techniques. Gating techniques are shown to be dependent on which parameters is chosen in reconstruction. Elastic motion correction does not involve choosing parameters, and is easy for the operator to perform. Dynamic frame based motion correction shows some improvement in volume estimation, but is far from as good as the existing techniques, however, some improvements can be done to this technique. Dynamic frame based gating shows promising results in both volume estimation and activity measurements, however, more experimentation needs to be conducted to further verify the effectiveness of the technique.

Acknowledgements

Above all, I would like to thank my supervisors Svein Jacobsen, Samuel Kuttner and Ola Engelsen for all support, interesting discussions and invaluable guidance they have provided. I am especially grateful for all the time Ola have given, staying late at work to help complete scanning and reconstruction.

I express my gratitude to my life-partner Julia Samuelsen for all the motivation and understanding she has provided. She had to take most of the work watching over our son as I have worked with this study late at night.

Finally I need to thank my office companion Daniel Henry Hansen for all the discussions and insights he have provided.

Stian Bakkevoll
Tromsø, June 2019

Contents

List of Figures

List of Tables

List of Abbreviations

^{18}F Fluorine-18

^{68}Ge Germanium-68

AC Attenuation Correction

bpm Breaths per Minute

CT Computed Tomography

DFG Dynamic Frame Gating

DFMC Dynamic Frame Motion Compensation

FWHM Full Width at Half Maximum

IQ Image Quality

LOR Line of Responce

MR/MRI Magnetic Resonance Imaging

MRAC MR Based Attenuation Correction

NAC Non Attenuation Correction

NEMA National Electrical Manufacturers Association

PET Positron Emission Tomography

SNR Signal to Noise Ratio

SUV Standardised Uptake Value

1

Introduction

Cancer is a major cause of mortality worldwide, with approximately 14 million new cases and 8 million cancer-related deaths in 2012. Lung cancer is the most frequent type of cancer with 13% of total cancer incidence, and is the leading cause of cancer-related deaths with 20 % of total cancer mortality in 2012[21]. Early and accurate staging of lung cancer is important in treatment selection, e.g. surgery, chemotherapy or radiotherapy [19].

Positron Emission Tomography (PET) is an important diagnostic tool in cancer staging and treatment decision making [19]. When PET is used to diagnose and stage lung cancer, it is highly effected by the motion induced by the patient breathing, causing motion blur [8]. Important parameters like Standardised Uptake Value (SUV) and tumour volume are under or over estimated due the motion[4].

To combat the effect of breathing motion, different techniques have been developed using combined PET/MR. These tools include elastic motion correction and different gating methods [6].

The aim of this study is to compare and study the impact of estimated tumor SUV and volume by using different correction/compensation methods, including elastic motion correction, optimal gating and amplitude based multi gating. Existing techniques require external components to perform motion correction or gating. Development of dynamic frame based compensation will be attempted to reduce the reliance of external components.

By comparing existing correction methods and developing new strategies, the hope is to advance the possibility of motion correction in PET reconstruction, and make it easier for operators to choose the best correction method in PET acquisition.

1.1 Thesis Structure

This thesis is divided in six chapters including Introduction.

Chapter 2 presents background material relevant to the study. The chapter provides an introduction to lung cancer, including the prevalence of cancer in Norway and cancer-related deaths. A brief overview of PET is presented explaining the working principles and the problems relating to breathing motion. The chapter contains a brief explanation of the breathing cycle and the different respiratory phases. Finally different motion correction strategies are presented, explaining the outline of each strategy.

Chapter 3 presents the materials and methods used in this study, explaining the working process in constructing a moving platform to induce motion in a phantom. The scanning procedure, reconstruction and analysis is explained in this chapter.

Chapter 4 presents the results from three different scans, containing measurements of estimated width and maximum activity.

Chapter 5 presents a discussion of the findings presented in chapter 4.

Chapter 6 presents a summary of the work and discusses the impact of this study. Finally future work is proposed to improve the results and advance the techniques presented in this study.

2

Background

2.1 Lung Cancer

Lung cancer was the most frequent cause of cancer-related deaths in Norway in 2017, reporting 2 234 deaths, followed by colon cancer with 1 178 deaths [18].

In 2017 there where reported 33 564 new cases of cancer in 32 740 individuals. Comparing the five year periods 2005-2012 and 2013-2017, we see an overall increase of 0.9 percent of new cases in men, and 5.5 percent in women [18].

Breaking down into different types of cancer, these where the most frequent types of new cases in 2017 in Norway: Prostate (4 983 cases), breast (3623 cases), lung (3 214 cases) and colon (3 007 cases) [18].

Lung cancer shows a low survival rate, reporting a 17.8 percent relative survival rate[1] after five years in the period 2013-2017[2]. Even lower rates are reported for lung cancer with proliferation showing a relative survival rate of 2.0 percent for distant proliferation [18].

1. The relative survival rate accounts for expected natural deaths for each age group.
2. By the time the report [18] was written, the mortality data for 2017 was incomplete, and is probably under reported.

2.2 Positron Emission Tomography

Positron emission tomography (PET) is a diagnostic tool that measures physiological function such as blood flow and metabolism through the means of a radiolabelled drug or tracer [2].

PET is based on detection of radioactivity emitted after the patient is injected with a small amount of the radioactive tracer [2].

Different tracers can be used, however they all include a positron emitting isotope. The emitted positron travel a small distance until it collides with an electron and annihilate, creating two gamma rays travelling in almost exactly opposite directions (180°) [13].

Arrays of detectors formed in adjacent rings compose the PET camera. When a gamma ray hits one of the detectors, the event is given a time stamp, and sent to the digital coincidence processor. After a fixed time, each event in the buffer is tested for coincidence with every other event by comparing the difference in detection time to a predetermined coincidence window. When two events are determined to be within the coincidence window, the coordinates of the line of response (LOR) is calculated for the coincidence event. Alternatively, the event information (detection time, position and energy) is stored in a list mode file for later reconstruction [13].

Multiple parallel LORs are combined to produce a single projection. Several of these projections are used to tomographically reconstruct a PET image, indicating the radiotracer distribution in the body.

In PET, the events originating from the edge of the subject has a higher possibility of being detected, resulting in a difference detected events depending on origin position. To compensate for this, attenuation maps are constructed using computed tomography (CT) or MR to estimate the attenuation throughout the subject [15, 20].

Figure 2.1 illustrates how events are registered in PET. [17].

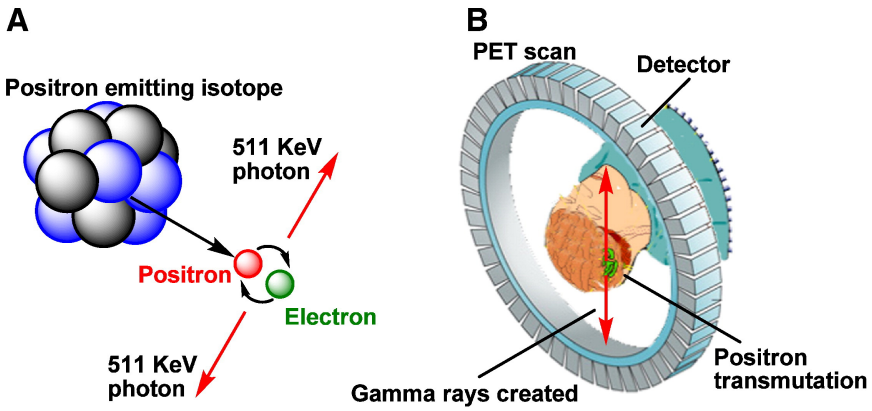

Figure 2.1: Figure illustrating the principle of PET. A positron is emitted from a positron emitting isotope and annihilated with an electron creating two gamma rays travelling in opposite direction. B The gamma rays are detected by the rings forming the PET camera.

2.3 PET in Lung Cancer

PET is frequently used in staging of lung cancer. However, motion caused by the patient breathing causes problems PET quality.

Breathing induced motion highly impacts the quality of PET images. Motion blur impacts important parameters such as SUV and lesion volume. Respiratory motion cause underestimation of SUV_{Max} and overestimation of lesion volume. Phantom and simulated studies indicates an underestimation of 28 % of SUV_{Max} and 130 % overestimation of lesion volume [4, 8]. These factors are important when SUV and volume derived from SUV thresholding are used in treatment decision making [8, 3].

2.4 Breathing motion

The breathing cycle consists of two phases, inspiration/inhalation and expiration/exhalation. Together the two phases form the respiration curve. Both phases is approximately of the same length. The respiration curve may vary between cycles, both in amplitude and period. The expiration phase is normally shorter than the inhalation phase.

During inspiration, the diaphragm contracts into the abdomen, making room for the lungs to expand. This results in a pressure difference allowing air to

flow into the lungs. The intercostal muscles between the ribs enlarges the chest cavity, resulting in expansion of the chest. For expiration, the opposite occurs [1].

In a study made by Kaneko and Horie (2012) [14] measuring breathing motion of the chest and abdomen, the movement was measured to be between 2.21–3.25 mm at the xiphoid during quiet (normal) breathing and 26.67–31.24 mm during deep breathing. Movements at the abdomen where substantially bigger, measuring between 8.07–10.85 mm.

The respiratory rate is normally between 12 to 20 breaths per minute (bpm) in adults under normal conditions. During breathing, the chest expands and retracts similarly for each breath [23].

Figure 2.2 illustrates each part of the breathing cycle in the form of an recording of a sleeping adult. In this example, one can see that the period of one cycle is about 4.5–5 seconds, yielding approximately 13 bpm, which is within normal respiratory rate. This example is only used to show the different parts of the breathing cycle and does not show the smaller variations of the respiratory curve.

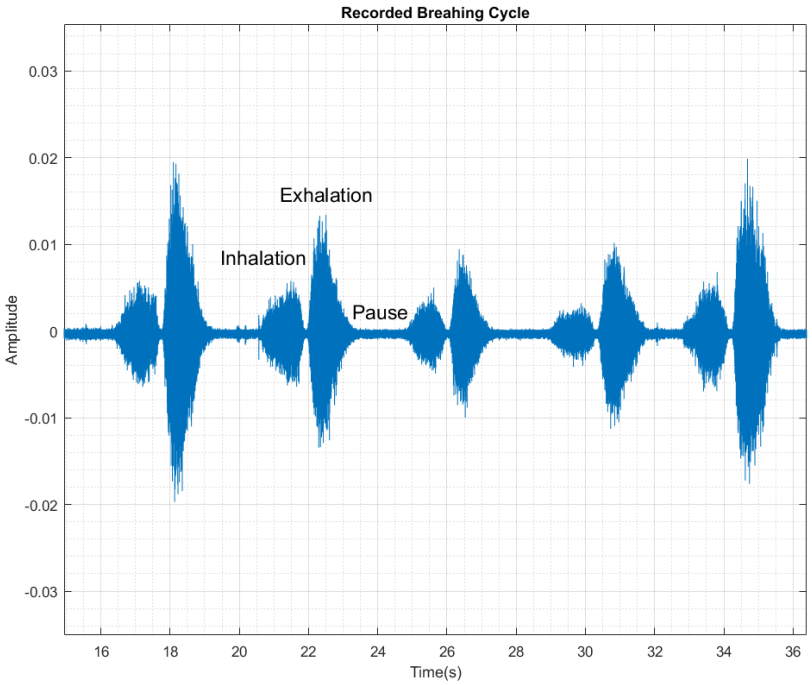

Figure 2.2: Recording of breathing by sleeping adult

2.5 Motion Correction Strategies in PET/MR

To be able to stage lung cancer correctly, and give the correct treatment, we need to correct for the motion induced by breathing. There exist different motion correction techniques commercially available today. This section will list some of these techniques.

2.5.1 Elastic Motion Correction

Elastic motion correction is an MR based correction strategy, and consists of three phases. In phase I, the MR based attenuation correction (MRAC) map is generated. This is usually performed before PET acquisition[9]. Phase II consists of a MR motion model scan. A self gating signal is acquired using 3D radial stack-of-stars in MR acquisition, meaning radial k-space sampling. This implies continuous smpling of the centre of k-space, which allows for detection of respiratory motion, resulting in a self gated signal [10, 11]. The self gated signal is correlated to the cushion signal which is placed on the patients chest to enable use the correction strategy after the radial stack-of-star MR sequence is completed.

The next step is to perform motion modeling. The MR raw data is segmented into bins according to the respiratory phases in the self gated signal. MR images are reconstructed from each segment. By using non-rigid registration algorithms, two sets of motion fields can be estimated. One to warp the expiration state to all other states, and the other to warp all other states to the expiration state. The attenuation map is then warped into the each other state, and PET is reconstructed. Finally the PET images are warped back to the expiration state [11].

In phase III, other diagnostic MR sequences are performed parallel to PET. In this phase, only the cushion signal is used to determine respiratory phases, and the motion model is used based on this signal for the rest of acquisition [9].

Figure 2.3 shows an overview of elastic motion correction [9].

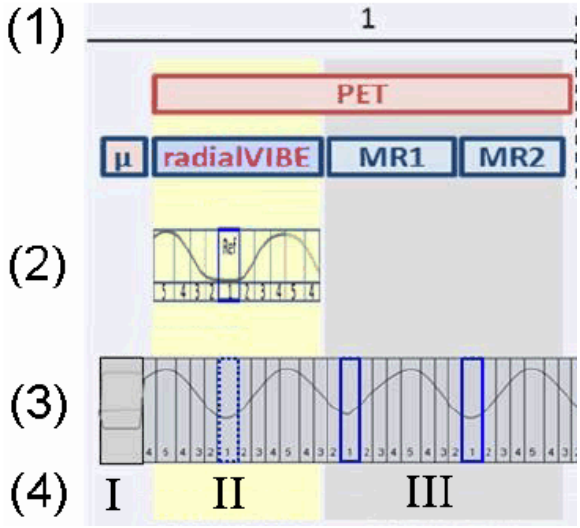

Figure 2.3: Illustration of elastic motion correction. (1) PET is acquired during phase II and III. (2) Selfe gating signal is acquired by radialVIBE. (3) Respiratory signal from cushion. (4) Phases. [9]

2.5.2 Gating

Optimal Gating is an amplitude-based gating strategy. The technique is based on amplitude histogram, and only utilizes the part of list mode data which have the least motion. [7, 12, 22]

The respiration curve generated form the cushion is analysed to determine the optimal gating sequence. An upper and lower threshold form an efficiency window. The size of the efficiency window can be manually selected in form of percentage, indicating the portion of list mode data used in reconstruction. The computer adjusts the thresholds until the efficiency window is as small as possible, indicating the lowest range of respiratory motion. This is illustrated in Figure 2.4 [22, 9].

Other gating techniques utilizes multiple gates at each respiratory cycle, partitioning the cycle into multiple phases or gates and reconstruction of attenuation maps for each phase. The placement of the gates can be based on time, amplitude or phase. The number of gates (n) can usually be decided in the scanner software [9].

Time Based Gating is performed by dividing the time axis into n equal lengths for the whole period of the breathing cycle, resulting in n gates. [9]

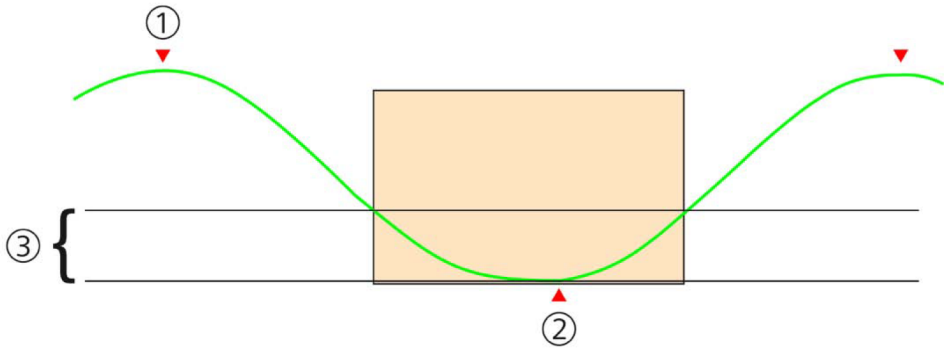

Figure 2.4: Optimal gating. 1:Inspiration phase, 2: Expiration phase, 3: Efficiency window. The marked area illustrates the gate location. [9]

Amplitude Based Gating is done by dividing the amplitude range into n/2 equal sections. The gates are then determined by dividing the time axis into n corresponding sections[3] [9].

Phase Based Gating divides the respiration curve into two phases, one inspiration phase, and one expiration phase. The n gates are then formed by dividing the time axis into n/2 equal length sections for each phase [9].

Illustrations of the different gating bases can be seen in Figure 2.5 [9].

2.5.3 Breath Hold

In early days, breath hold was the only available technique to combat breathing motion. This is the best way to reduce motion blur in images, and is therefore still used in CT, and fast MR sequences such as MRAC. However, PET acquisition is performed over several minutes, which makes breath hold impossible in PET and long MR sequences.

2.5.4 Dynamic Frame Based Motion Correction and Gating

Dynamic frame based motion correction (DFMC) and dynamic frame based gating (DFG) are two proposed strategies developed in this study. Both are based on dynamic reconstruction from list mode data into short frames. From these frames, the relative frame x,y-position is estimated by using a weighted average of all the slices in each frame.

3. The time axis is divided into sections where the respiration curve lies inside the boundaries of the corresponding amplitude section.

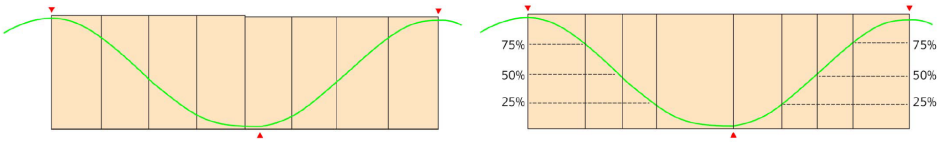

(a) Time based gating

(b) Amplitude based gating

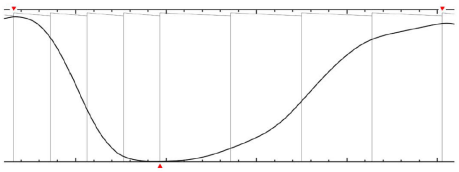

(c) Phase based gating

Figure 2.5: Illustration of time, amplitude and phase based gating. (a) Time axis is divided into sections of equal length, resulting in gates for expiration and inspiration respectively. (b) The amplitude range is divided into equal sections. The gates are determined from the corresponding sections along time axis. The figure shows four different amplitude sections resulting in eight different gates. (c) The respiration curve is divided into one inspiration phase and one expiration phase. The gates are determined by dividing the time axis into equal lengths for each phase. [9]

In DFMC each frame is moved to a reference frame position, rounded to the nearest pixel. The reference frame used in this method is the frame with lowest estimated y position. All frames are then summed together, and appropriately scaled with respect to the total number of frames.

DFG uses the position information to gate the signal. All frames which lie within a tolerance position window is summed together and scaled with respect to number of frames used. The rest of the frames are either discarded or reconstructed in other bins.

3

Materials and Method

3.1 Construction of Moving Platform

To study the quality of motion correction and gating strategies, it is desirable to have reproducibility, as well as a ground truth to compare the results to. This can be accomplished by construction of a moving platform. This platform needs to be constructed to fit a phantom in a Siemens Biograph mMR integrated PET/MR scanner. In this study, two different phantoms are used, i.e. the National Electrics Manufacturers Association Image Quality (NEMA IQ) water phantom and Germanium-68 (^{68}Ge) rods submerged in water. These phantoms weigh 10 and 5 kg respectively.

The platform needs to be constructed as part of the thesis, and therefore needs a relatively simple design in order to complete the platform in sufficient time. There is no specified budget for the thesis, which means the costs needs to be held at a minimum.

The platform must meet the following requirements:

- Platform area of 400 mm × 400 mm
- Support a phantom up to 10 kg
- Approximately 20 mm vertical motion

- Motion similar to human breathing
- Non magnetic
- Low cost
- Simple design

3.1.1 Design

The design of the moving platform needs to meet many requirements resulting in few possible designs. An electric design would be ideal, but contains magnetic parts and is not suitable for use in an integrated PET/MR machine due to strong magnetic fields, as well as induced artefacts in MR images.

A hydraulic design would introduce further attenuation resulting in lower signal to noise ratio and may cause leak spillage.

A mechanic design would be possible, but requires actuation from close proximity to the scanner which is not ideal due to loud noise, and the fact that scanning is initiated from outside the room containing the scanner. Communication with the operator would in this case be difficult.

To meet all the requirements, it was decided to construct a pneumatic system using multiple bellows, as illustrated in Figure 3.1. The design contains a platform with four equal bellows pushing on a plastic plate with a phantom placed on top. A fifth bellow is placed outside the scanner room, driving the four bellows inside the MR machine, in turn moving the platform and phantom.

The advantage of using a four to one bellow system is reduction of force needed to lift the phantom by taking advantage of Pascal's Law [24]. This entails that the force needed on the driver bellow to lift a 10 kg phantom is about 2.5 kg. In order to lift the phantom 20 mm, the driver bellow needs to be compressed 80 mm.

An automated system was considered, using a motor to push the driver bellow, however, the design would be much more complex and time consuming. It was therefore decided to actuate the system manually, by hand pushing the driver bellow, following the breathing cycle of the person pushing the bellow.

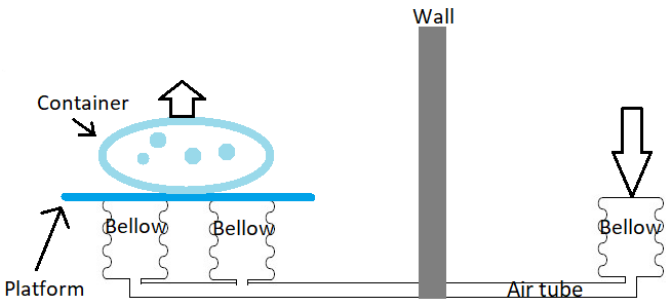

Figure 3.1: Design of moving platform constructed of bellows.

3.1.2 Construction

Parts needed for construction:

- 5 Bellows
- 10 m air hose
- 3 Plexiglas (400 mm × 400 mm) plate
- MS Polymer sealant

The main problem to solve with this simple design, is to transfer the air from the driver bellow to all four driven bellows simultaneously. This is accomplished by using the air hose as a spacer between two Plexiglas plates. The plates were then sealed together with MS Polymer to make the construction air tight. Four holes were drilled at the corners of one of the plates where the bellows are going to be mounted.

Each of the four driven bellows were then sealed over each hole. A cap was finally sealed at the top of each driven bellow allowing the third Plexiglas plate to be placed on top, forming the platform. The platform itself was not glued to the bellows, and is resting freely on top.

The driver bellow was sealed at both ends. A hole was drilled at one end in order to mount the hose connection. The hose can not be fitted permanently to the driver bellow, as the hose needs to be fed through a hole in the wall. The connection is a tap which the hose is threaded on to, and fastened with a hose clamp.

An image of the construction is found in Figure 3.2.

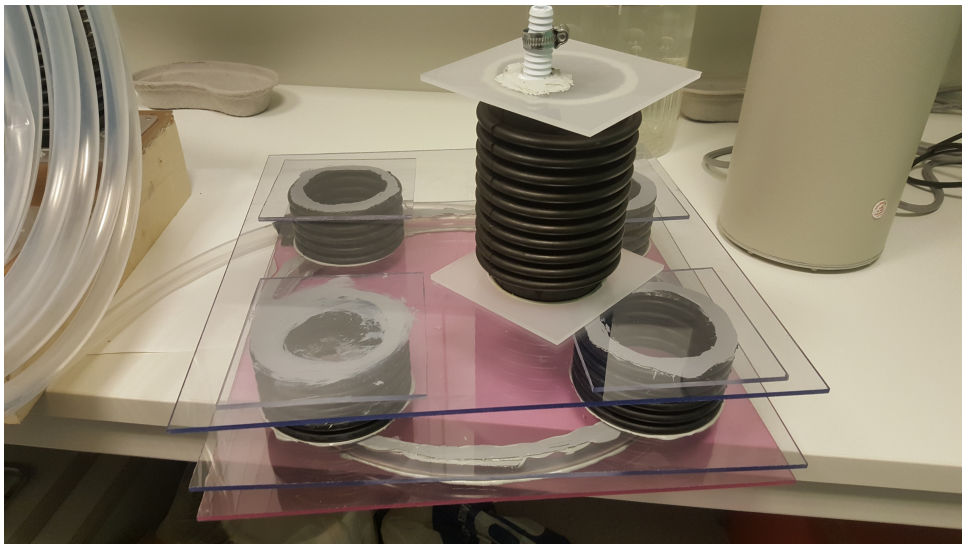

Figure 3.2: Image of the constructed moving platform.

3.2 Phantoms

The NEMA IQ phantom consists of a water tank with six submerged isolated spheres (inner diameters 37, 28, 22, 17, 13, and 10 mm)[26]. The four smallest spheres were then filled with the tracer (^{18}F) to simulate a tumour, while the rest were filled with pure water. The surrounding water contained a more dilute tracer to simulate background. The tracer concentrations were measured to be 0.104 MBq/ml in the spheres, and 0.0296 MBq/ml in the surrounding water at the time of measure. The total weight of this phantom is approximately 10 kg. Figure 3.3 shows an image of this phantom.

The ^{68}Ge phantom is water-filled container, with two (3.5 mm diameter) rods containing the tracer (^{68}Ge) submerged. The water in this phantom is pure (containing no tracer). The total weight of this phantom is approximately 5 kg. An image of this phantom is shown in Figure 3.4

Figure 3.3: Image of NEMA IQ phantom

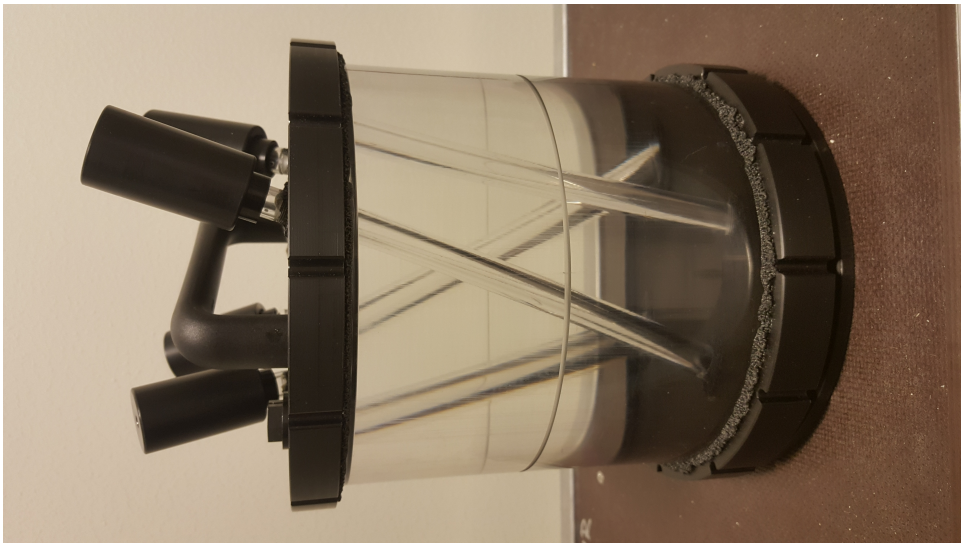

Figure 3.4: Image of ^{68}Ge phantom

3.3 PET/MR Scanning

There exists commercial tools for correcting breathing induced motion blur in PET images, e.g. Siemens HD•Chest (optimal gating), Siemens Multi Gate (multiple time, amplitude and phase based gating) and Siemens BodyCOMPASS (elastic motion correction).

Multiple scans were performed using the two phantoms, i.e. NEMA IQ, and ^{68}Ge-rod. The phantoms were placed on the constructed platform, and placed in a Siemens Biograph mMR combined PET/MR scanner.

In total five MR sequences in addition to PET was performed during scanning to obtain structure, attenuation map and enable Siemens BodyCOMPASS. The following sequences where performed:

- MRAC
- StarVIBE BodyCOMPASS
- T1 weighted StarVIBE
- Two trigger based sequences
- PET acquisition

A total of 11 scans were made. Significant leakage from the platform system was a major problem in many scans, which are excluded from the study. Three of the datasets where selected and used for further processing. The datasets are numbered from 1 to 3 in this study.

Dataset 1 was obtained using the ^{68}Ge phantom. The moving platform was driven at an amplitude of 3 mm, following normal respiration frequency. The platform was driven manually by following the real time breathing cycle of the person driving the system. The total PET acquisition time was 1 181 seconds.

Dataset 2 was obtained using the ^{68}Ge phantom. The moving platform was driven at an amplitude of 18 mm. The respiration period was extended to approximately 3 seconds for each phase. This was done due to limitations on dynamic reconstruction in the RetroRecon tool available in the scanner software, as the software only allowed for frame duration as low as 3 seconds. This is done to simulate 1 second frame duration in dynamic reconstruction. The platform was driven by blowing into the air hose to maintain pressure, as the system was leaking air under higher pressure. The total PET acquisition

time was 650 seconds.

Dataset 3 was obtained using the NEMA IQ phantom. The moving platform was driven at an amplitude of 18 mm, following normal respiration frequency. The platform was driven by blowing into the air hose to combat leakage, following a respiration frequency of approximately 14 bpm. The total PET acquisition time was 1 261 seconds.

An overview of the scanning parameters are shown in Table 3.1.

Table 3.1: Scanning parameters for each dataset.

Dataset	Phantom	Acq. time [s]	Motion amp. [mm]	Resp. period
1	^{68}Ge	1 181	3	Normal
2	^{68}Ge	650	18	Extended
3	NEMA IQ	1 261	18	Normal

3.4 Image Reconstruction and Processing

The PET data was reconstructed using the RetroRecon tool in the scanner software (Siemens syngo MR E11P). Reconstruction were made using HD•Chest, Multi Gates, BodyCOMPASS and Dynamic reconstruction.

HD•Chest were reconstructed using a 50 % efficiency window for all three datasets.

Reconstructions using Multi Gates were done differently for all datasets. Different amounts of gates were used to try optimizing with respect to the respiration curve. All datasets were reconstructed using amplitude based gating. Six gates were used in reconstructing dataset 1, four gates in dataset 2 and eight gates in dataset 3.

Dynamic reconstruction was done using three second frames. 10 frames were reconstructed in dataset 1, 30 frames in dataset 2 and 40 frames in dataset 3. The complete signal was not used in dynamic reconstruction, as the total amount of data would be to big for processing due to computer memory limitation.

The effectiveness of each of these tools was investigated and compared. New method were be attempted, using dynamic reconstruction of the list mode data from PET acquisition, without the use of external sensors or scanners, i.e DFMC and DFG.

Dataset 1 was not processed using DFG. Due to underestimation of motion, most of the frames would lie inside the tolerance window, effectively resulting in an uncorrected image.

Dataset 3 was not processed using either DFMC or DFG. A combination of too few frames and low SNR results in images where the spheres are not detectable.

All processing is done using the Siemens syngo MR E11P software and Matlab R2018b.

3.5 Image Analysis

The values of maximum activity were measured for one of the ^{68}Ge rods in dataset 1 and 2, and for the largest sphere in dataset 3. This was done by importing the images into Matlab and scaled according to the "RescaleSlope" parameter in the header file. The maximum activity within the rods and spheres was then recorded. The maximum activity is directly proportional to SUV [16].

The width of the rods and spheres were estimated by calculating full width at half maximum (FWHM). This was done by importing the images into ImageJ and plotting the line profile trough the rod and sphere. This was done for the same slice at each reconstruction.

The ^{68}Ge rods are quite narrow(3.5 mm), and appears as a point source in the reconstructed images. To give a better estimate of the FWHM, a gaussian profile is fitted to the line profile, and the FWHM is calculated from the estimated standard deviation. This is performed in the built in curve fitting tool in ImageJ. An illustration of the curve fitting process is illustrated in Figure 3.5.

Dataset 3 was analysed using both the attenuation corrected (AC) and non attenuated correction (NAC) reconstructions. Imaging the NEMA IQ phantom filled with water on a 3.0 Tesla MR system, leads to artefacts and signal inhomogeneities due to standing-rf-wave phenomena and T1 effects [26, 25]. This affects the MRAC based attenuation map used in AC reconstruction, and degrades the reconstructed PET image quality.

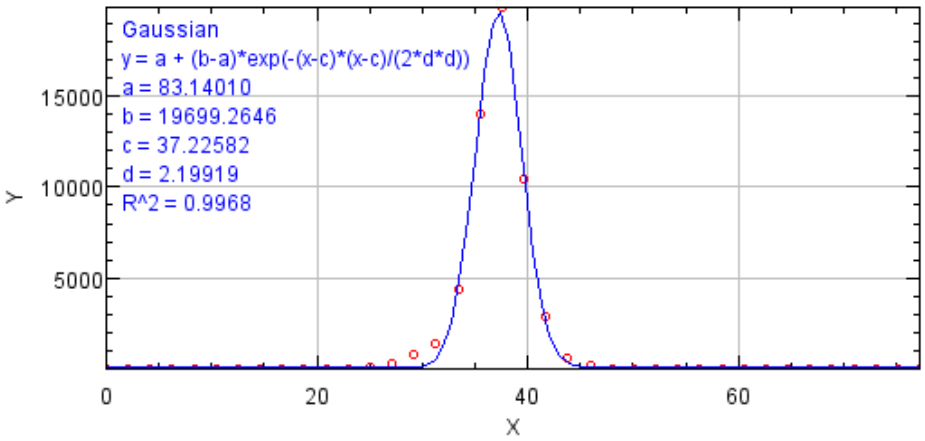

Figure 3.5: Illustration of a gaussian fit to line profile.

4

Results

4.1 Dataset 1

4.1.1 Width Measurements

Tables 4.1 and 4.2 shows the measured width of the ^{68}Ge rods from dataset 1 and 2. The width is based on FWHM. The uncorrected reconstruction shows an estimated width of 4.6 mm.

The DFMC reconstruction gives the same result as uncorrected. Due to a low estimated motion, only one frame is moved one pixel down, resulting in a minimal change with respect to the uncorrected reconstruction. The estimated motion can be seen in Figure 4.1.

The BodyCOMPASS reconstruction shows a significant decrease of 0.8 mm with respect to uncorrected reconstruction, resulting in a measured diameter of 3.8 mm.

Multi Gates reconstruction show varying results between 4.5–5.0 mm. Only gate 6 indicates a smaller width then the uncorrected reconstruction. These results may have been improved by increasing the number of gates, resulting in a lower amplitude variation within each gate.

HD•Chest reconstruction also increases the estimated width of the rod, measuring 4.9 mm. This could probably be decreased by using a smaller efficiency

window then 50 %.

Table 4.1: Calculated FWHM for the different reconstruction methods on dataset 1 and 2.

	FWHM [mm]	
Correction Strategy	Dataset 1	Dataset 2
Uncorrected	4.6	23.0
DFMC	4.6	14.7
DFG	-	4.5
BodyCOMPASS	3.8	5.2
Multi Gates	-	-
HD●Chest	4.9	21.6

Table 4.2: Calculated FWHM for each gate for the Multi Gates reconstruction on dataset 1 and 2.

	FWHM [mm]	
Gate number	Dataset 1	Dataset 2
1	4.9	21.3
2	5.0	4.4
3	4.7	21.3
4	4.8	5.8
5	4.8	-
6	4.5	-

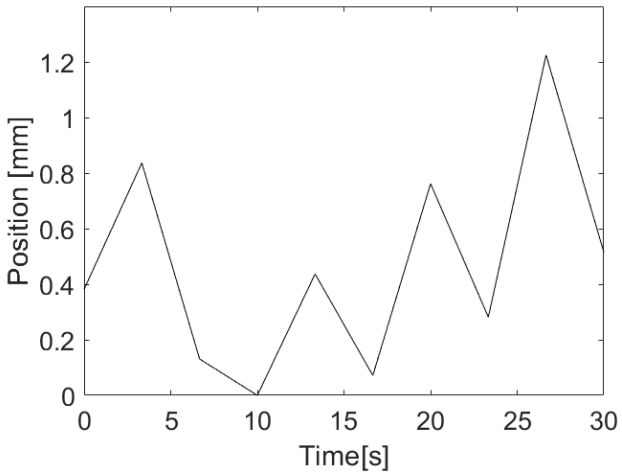

Figure 4.1: Estimated motion based on dynamic frames for dataset 1.

4.1.2 Maximum Activity Measurements

The activity measurements are shown in Figure 4.2.

The maximum activity measured in the uncorrected reconstruction shows an activity level of 2.12 MBq/ml.

BodyCOMPASS reconstruction shows the highest maximum activity with a measure of 2.34 MBq/ml.

HD•Chest reconstruction gives a maximum activity level slightly higher then uncorrected with a measure of 2.16 MBq/ml.

Multi Gates reconstruction gives varying activity results between 2.03 MBq/ml–2.20 MBq/ml. These results show both higher and lower activity levels then the uncorrected reconstruction. As each gate is reconstructed from different parts of the breathing cycle, one would expect these variations.

DFMC show a significant decrease in activity level with respect to the uncorrected reconstruction with a measure of 1.61 MBq/ml. The fact that DFMC only uses a small part of the list mode data may impact this result.

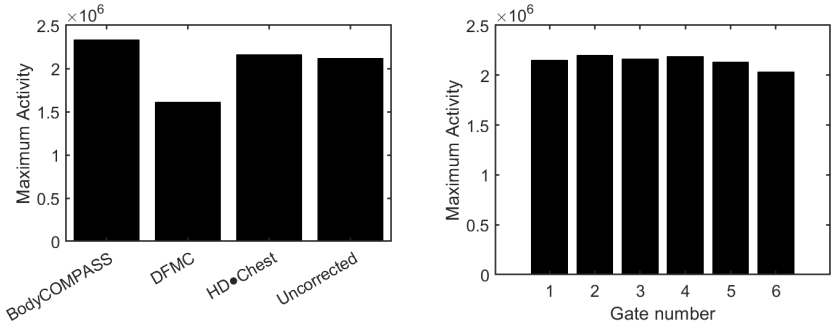

(a) **(b)**

Figure 4.2: Measurements of maximum activity in dataset 1. (a) Maximum activity of BodyCOMPASS, DFMC, HD•Chest and Uncorrected reconstruction. (b) Maximum activity of Multi Gates reconstruction.

4.2 Dataset 2

4.2.1 Width Measurements

Uncorrected reconstruction indicates a FWHM of 23.0 mm, which is far from the true value of 3.5 mm. This indicates a big impact of motion during acquisition.

Using DFMC reconstruction reduces the measured width to 14.7 mm, still showing high motion corruption. As the respiration period is extended, each frame contains less motion. The estimated motion has an amplitude of approximately 15 mm, which is close to the actual 18 mm amplitude. Figure 4.3 illustrates the estimated motion.

DFG reconstruction show a great reduction of the measured FWHM, reducing the estimation to 4.5 mm.

BodyCOMPASS reconstruction reduces the measured FWHM down to 5.2 mm, a total reduction of 17.8 mm.

HD•Chest reconstruction reduce the estimated width, resulting in a FWHM measure of 21.6 mm. Again, this could have been greatly improved by reducing the efficiency window.

Multi Gates shows differing results, with a FWHM of 21.3 mm at gate 1 and 3, 4.4 mm at gate 2 and 5.8 mm at gate 4. This indicates that gate 1 and 3 are placed exactly on the expiration and inspiration slopes.

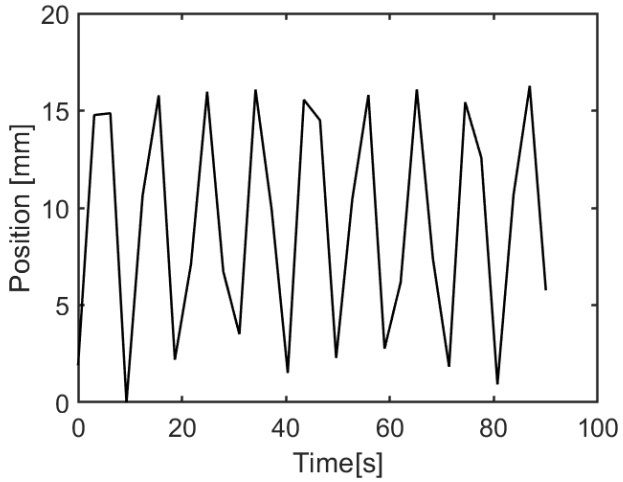

Figure 4.3: Estimated motion based on dynamic frames for dataset 2.

4.2.2 Maximum Activity Measurements

The measured activity for each correction method is shown in Figure 4.4.

Uncorrected reconstruction shows a maximum activity of 0.617 MBq/ml.

BodyCOMPASS reconstruction shows a large increase in maximum activity, measuring 0.802 MBq/ml.

HD•Chest reconstruction shows a very slight increase of 0.001 MBq/ml with respect to uncorrected reconstruction measuring 0.618 MBq/ml.

Multi Gates shows varying results in maximum activity, measuring between 0.446–1.31 MBq/ml. Figure 4.4 (a) clearly shows that gate 1 and 3 measures a very low maximum activity compared to gate 2 and 4. Gate 2 shows the highest measured activity level in this dataset, measuring 1.31 MBq/ml

DFMC reconstruction show a significant decrease in maximum activity measuring 0.394 MBq/ml.

DFG shows a significant increase in maximum activity compared to uncorrected reconstruction, measuring 0.964 MBq/ml.

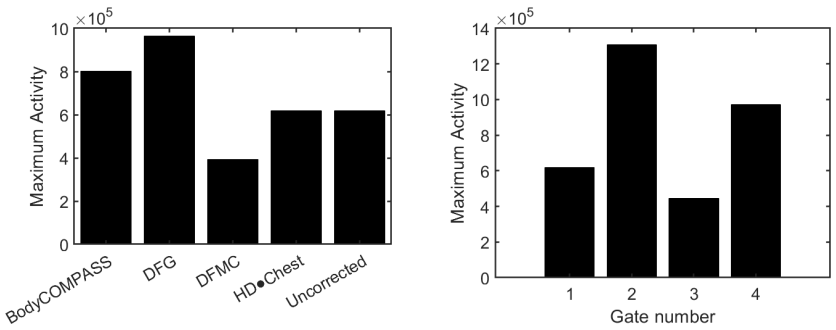

(a) **(b)**

Figure 4.4: Measurements of maximum activity in dataset 2. (a) Maximum activity of BodyCOMPASS, DFG, DFMC, HD•Chest and Uncorrected reconstruction. (b) Maximum activity of Multi Gates reconstruction.

4.3 Dataset 3

Measurements on dataset 3 are made for both AC and NAC reconstruction, due to artefacts in the attenuation map generated by the MRAC sequence

[25].

Figures 4.5 and 4.6 shows the detected movement using NAC and AC dynamic frames respectively. One can see the big impact of incorrect attenuation correction by the corruption in estimated motion between AC and NAC reconstructed frames.

DFMC and DFG was attempted, but due to computer memory restrictions only 40 three-second frames were able to be used in reconstruction. This entails that only 9.5 % of the list mode data was used in reconstruction, barely giving enough signal to detect the spheres but not to conduct measurements. The same issue was evident on the Multi Gate reconstruction, resulting in incomplete measurements, especially on the NAC reconstructions.

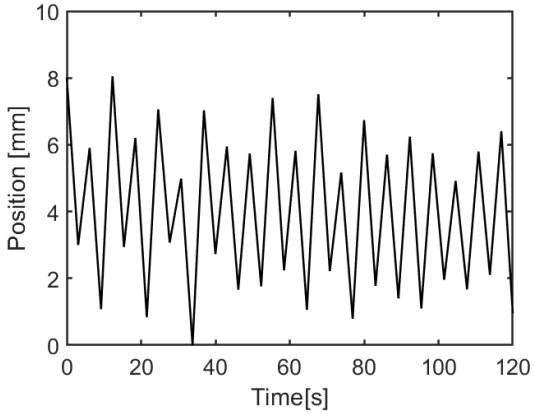

Figure 4.5: Estimated motion based on NAC dynamic frames for dataset 3.

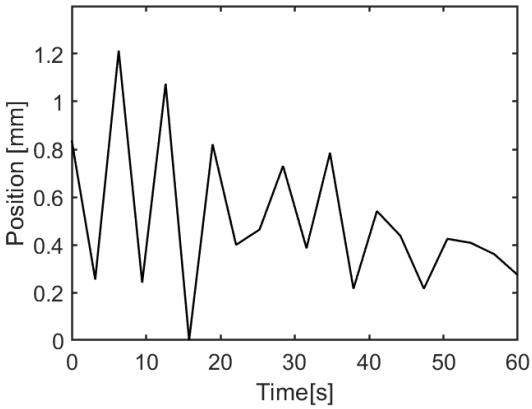

Figure 4.6: Estimated motion based on AC dynamic frames for dataset 3.

4.3.1 Width Measurements

Tables 4.3 and 4.4 shows the measured width of the three largest spheres containing activity. The smallest sphere had to low signal to give quality measures.

Uncorrected reconstruction measures the 22, 17 and 13 mm sphere to be 21.3, 16.1 and 14.2 mm respectively for the NAC reconstruction. AC reconstruction estimates 23.6, 15.5 and 16.0 mm respectively.

BodyCOMPASS utilizes attenuation correction in reconstruction, only allowing for AC reconstruction. The 22 and 17 mm spheres were measured to be 24.7 and 16.0 mm respectively. The 13 mm sphere had to low signal to detect.

HD•Chest reconstruction measures the spheres to be 20.6, 15.4 and 14.9 respectively in NAC reconstruction, and 23.3, 15.3 and 15.7 mm in AC reconstruction.

In the NAC Multi Gates reconstruction, only gate 5 showed enough signal to measure all tree spheres. The spheres were measured to be 20.1, 15.5 and 11.2 mm respectively. Gate 7 and 8 allowed for measurements on the 22 mm sphere, giving a measure of 22.3 and 21.3 mm respectively.

In tha AC Multi Gates reconstruction, all gates showed a sufficient amount signal to measure three of the spheres. The measurements differed between 17.9–25.5 mm on the 22 mm sphere, 12.3–16.4 mm in the 17 mm sphere and 13.7–17.9 mm on the 13 mm sphere.

Table 4.3: Calculated FWHM for each correction method except Multi Gates on dataset 3.

	FWHM [mm]					
	Not attenuation corrected			Attenuation corrected		
Correction strategy	22 mm	17 mm	13 mm	22 mm	17 mm	13 mm
Uncorrected	21.3	16.1	14.2	23.6	15.5	16.0
BodyCOMPASS	-	-	-	24.7	16.0	-
HD•Chest	20.6	15.4	14.9	23.3	15.29	15.72

Table 4.4: Calculated FWHM of each gate in Multi Gate reconstruction on dataset 3.

	FWHM [mm]					
	Not attenuation corrected			Attenuation corrected		
Gate number	22 mm	17 mm	13 mm	22 mm	17 mm	13 mm
1	-	-	-	21.9	13.4	14.5
2	-	-	-	21.2	14.3	17.0
3	-	-	-	17.9	12.3	15.6
4	-	-	-	23.0	14.8	16.0
5	20.1	15.5	11.2	22.5	15.0	13.7
6	-	-	-	24.6	15.0	14.9
7	22.3	-	-	25.5	16.4	17.9
8	21.3	-	-	21.7	14.6	15.5

4.3.2 Maximum Activity Measurements

The activity measurements of NAC reconstructions can not be compared to AC reconstructions or the actual activity concentration. The activity calculated by PET is highly dependent on attenuation correction to give accurate results.

Uncorrected reconstruction measures the maximum activity to be 0.0966 MBq/ml in the AC reconstruction, and 1.80 kBq/ml in NAC reconstruction.

BodyCOMPASS reconstruction show a decrease in maximum activity, measuring 0.0735 MBq/ml in AC reconstruction.

HD•Chest reconstruction show a decrease in maximum activity in the AC reconstruction, measuring 0.0881 MBq/ml. In NAC reconstruction, the maximum activity is measured equal to the uncorrected NAC reconstruction.

Multi Gates reconstruction show varying results in maximum activity, measuring between 0.0936–0.176 MBq/ml in AC reconstruction, and between 1.936–2.498 kBq/ml in NAC reconstruction. The results show an increase in maximum activity for all gates in NAC reconstruction. For AC reconstruction gates 5 gates show an increase in maximum activity.

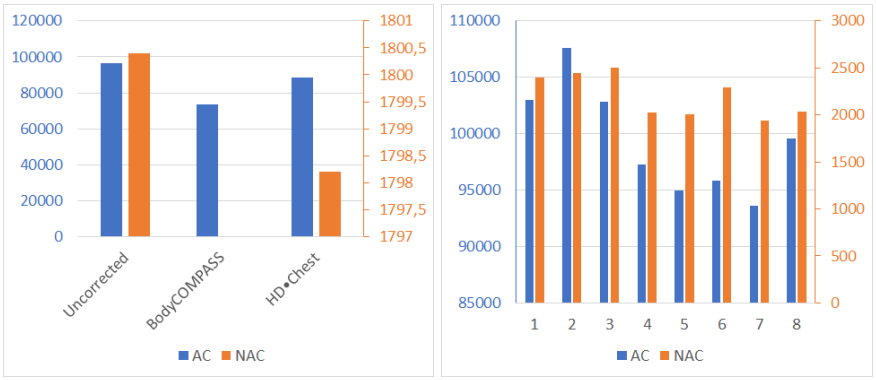

(a) **(b)**

Figure 4.7: Measurements of maximum activity in dataset 3. (a) Maximum activity of Uncorrected, BodyCOMPASS and HD•Chest. (b) Maximum activity of Multi Gates reconstruction.

5 Discussion

5.1 Dataset 1

5.1.1 Measured Width

Based on the width measurements, one would expect the width to be more narrow in the gated and corrected images. This is however not what we see form most of the gating based methods. Only the BodyCOMPASS and one gate from Multi Gates reconstructions shows a more narrow width of the rod.

BodyCOMPASS reconstruction show a width decrease of 17 %, which would translate into a 44 % volume reduction. This is a significant decrease, closing in on the real width of 3.5 mm. This measure is smaller then expected, as performance measurements done on Siemens Biograph mMR have shown a resolution of 4.3 mm [5].

Multi Gates reconstruction shows some varying results at the different gates, differing from a 2 % decrease to a 9 % increase in width, translating into a variance between a 6 % reduction to a 28 % increase in estimated volume. In general the widths are measured wider then for the uncorrected reconstruction with one exception. Why this is the case is not obvious, but might be due to gate positions in the breathing cycle. Choosing more gates may have shown better results from Multi Gates.

HD•Chest reconstruction show a 7 % increase in width translating to 21 %

increase in volume. The reconstruction was conducted with a 50 % efficiency window which is the maximum allowed by the software. By reducing the efficiency window we would probably see an improvement in this result, as the amplitude variation in the reconstructed data would be lower.

DFMC shows no reduction in width. By using the weighted average, one can clearly see periodic motion in the data. The motion is however underestimated. The real motion amplitude is known to be 3 mm, but the estimation shows about 1.2 mm motion amplitude. One would expect this underestimation, as each frame is three seconds long. This indicates that there are motion within the frames, which average out the position to indicate a lower amplitude. As the estimated motion is underestimated, most of the dynamic frames would not be corrected at all. However, this result may have been improved by implementing linear interpolation. This would allow us to move the frames by a smaller distance then one pixel.

5.1.2 Measured Activity

In the activity measurements, most gating and correction strategies increase the maximum activity with respect to the uncorrected reconstruction. There are only two measurements showing a decrease in activity, which is one of the gates in Multi Gates reconstruction and DFMC.

BodyCOMPASS reconstruction shows a 10 % increase in maximum activity with respect to the uncorrected reconstruction. This is in line with what is expected. When motion is "removed" from the image, the peak value should increase as the activity is concentrated in a smaller volume.

Multi Gates reconstruction show various results depending on which gate is considered. The activity measurements are generally higher than for the uncorrected reconstruction, differing from a 8 % decrease to a 4 % increase in maximum activity. Interestingly, the highest increase in measured activity correspond to the highest increase of measured width, and the highest decrease in measured activity correspond to the highest decrease in measured width. This indicates that the maximum activity impacts the measured width in an opposite manner than expected.

HD•Chest reconstruction show a very small increase in activity, measuring a 2 % increase. This result is surprising when compared to the width measurement, as the width is increased by 7 %. This show the same trend as for Multi Gates reconstruction.

DFMC show a significant decrease in maximum activity. The measured maxi-

mum activity is 24 % lower then for the uncorrected reconstruction. This is not expected at all, as the widths are measured equal. The fact that the reconstruction only uses part of the PET data may impact the result. It would be optimal to use the complete data, but this would demand higher computational power than what was available in this study.

5.2 Dataset 2

With a motion amplitude of 18 mm, we expect the widths to be significantly lower and the maximum activity to be significantly higher in the gated and corrected images compared to the uncorrected.

5.2.1 Measured Width

BodyCOMPASS reconstruction show a 77 % decrease in width, translating to a 99 % decrease in estimated volume. With a high motion amplitude throughout the acquisition, this is expected, and shows a great improvement.

Multi Gates reconstruction again shows different results depending on which gate is considered. This is what is expected as some of the gates will be placed in more varying positions in the breathing cycle. Two of the gates show high reduction of width, indicating that these gates have low motion corruption. These gates show 80 % and 75 % reduction in width. This would translate to a volume reduction of 99 and 98 %.

HD•Chest show a 6 % decrease in width, translating to 17 % decrease in estimated volume. This is not a large reduction of width, as other strategies showing far grater reduction. Again, decreasing the efficiency window might improve the result significantly.

DFMC results in a 36 % reduction of width, translating to 74 % reduction of estimated volume. This is still far from the ground truth of 3.5 mm, and shows lower performance than other strategies. We can see that the estimated motion is still underestimated, but with a much lower factor then in dataset 1. The motion appears smother, however the low frame-sampling frequency still is a big problem.

DFG results in an 80 % decrease in width, translating to 99 % reduction in estimated volume. This is far better then most other strategies, only beaten by one gate in Multi Gates reconstruction. This result show some promising potential of dynamic frame based gating.

5.2.2 Measured Activity

BodyCOMPASS results in a 23 % increase in maximum activity. As expected, this is a significant increase in the measured maximum activity. This result show that BodyCOMPASS can handle large movements.

Multi Gates again show varying results. We see an 112 % increase in maximum activity at gate 2, and 58 % increase at gate 4. Gate 1 shows more or less the same result as the uncorrected reconstruction, and gate 3 show an decrease in maximum activity. In this experiment an increase in maximum activity corresponds to decrease in width, which is in line with what we expect.

HD•Chest results in more or less equal maximum activity as for the uncorrected reconstruction, showing an increase of only 0.6 %. We would expect a more significant increase after the gating. Again we can see that a 50 % efficiency window is to large to reduce motion corruption sufficiently.

DFMC show a significant decrease in maximum activity. The problem in this experiment is the frames which lies between the upper and lower position. Much of the activity in these frames are averaged with zero, resulting in an overall decrease in activity.

DFG show a significant increase in measured activity, indicating a 56 % increase in maximum activity. This method shows promising potentials in reducing motion corruption, however only one of the experiments were suitable for DFG. More experimentation would need to be done to see the complete of this method.

5.3 Dataset 3

Due to the standing-RF-wave artefacts resulting in an incorrect attenuation map, it is difficult to obtain reasonable results in AC reconstructions. For this reason, the AC reconstructions will not be considered in this discussion. As BodyCOMPASS is MR based, and only allows for AC reconstruction, this method can not be considered in this experiment. However the results from these reconstructions are included in chapter 4.

This dataset has a low SNR, making it difficult to preform width measurements on the reconstructed images. One problem is that the NAC reconstruction overestimates the activity originating from the phantom edges, resulting in an even lower SNR then what is expected.

As the SNR is very low, when gating is performed and we do not use all of the list mode data, the spheres are barley visible. This gives incomplete results and no value to this study.

5.4 Summary

The results clearly show that motion has a high impact on PET images. The width and maximum activity is highly effected.

The results of the experiments show that gating is highly dependent on many parameters, i.e. efficiency window, number of gates, and gate positioning. However when the parameters are properly chosen, great improvements are made.

Elastic motion correction (BodyCOMPASS) seams like a more stable technique, not dependent on many parameters. The problems faced in dataset 3 does not occur in real patients, and is strictly due to the fact that the phantom is filled with pure water.

DFMC does show some possibilities when it comes to width measurements, but makes activity measurements worse. However by introducing interpolation, the results could be improved. There are also possibilities of dividing the frames into different segments, and estimate the movement of each segment. This must be done to combat movements in different directions.

DFG show promising results, improving the width and activity measurements. This might be a suitable technique when only PET data is available. However, dividing the data into multiple frames requires a lot of computational power to process. The technique is only tested in one experiment as the other where not suitable. The quality of these results needs to be controlled with other experiments.

6 Conclusion

6.1 Summary

PET images are highly impacted by respiratory motion during acquisition. The aim of the study was to compare different correction strategies available in PET/MR reconstruction. Two new strategies where attempted and compared to the existing tools available.

A moving platform was constructed to induce breathing movement to different phantoms, i.e. NEMA IQ and ^{68}Ge rods. The phantoms were placed on the platform and scanned with Siemens Biograph mMR, combined PET/MR.

PET images were reconstructed using Siemens BodyCOMPASS, HD•Chest, Multi Gates and Dynamic Frames. From the dynamic frames, one correction method and one gating method where introduced to compensate for motion.

Three experiments were conducted. Two using the ^{68}Ge rods phantom with different motion amplitude and period, and one using NEMA IQ.

BodyCOMPASS seamed to be a stable correction method, showing significant improvement on both size and activity level. The technique works well for both high and low motion amplitude, and is not effected by the motion period.

Gating methods show some difficulties in deciding parameters such as number

of gates, efficiency window and gate positioning. However, when appropriately chosen, the results may show significant improvement on both size and activity level.

DFMC show some possibilities, but still needs a lot improvements. The activity level is highly suppressed by using this technique, but may show improvements in size measurements.

DFG shows a lot of possibilities, but needs to be quality controlled. The technique is only done in one experiment, but shows significant improvement in both size and activity measurements.

6.2 Impact

The results of this study indicates that elastic motion correction is superior to existing gating techniques. Elastic motion correction is by far the easiest and fastest technique for the operator to choose, and show better results then most gating techniques.

The study shows that dynamic frame based techniques are possible, with dynamic frame based gating showing promising results. These gating techniques are not reliant on external equipment, but still allowing decent reconstructions. However, the attenuation map is still required, and calls for the use of either MR or CT to obtain the map.

This study will hopefully help operators choose which correction strategy to use for PET reconstruction.

6.3 Future work

To have more control of the motion parameters, the motion induced by the moving platform should be automated. This would increase reproducibility, and enable more control of motion amplitude, frequency and make sure that the platform moves in a realistic respiratory motion.

Further work on the DFMC and DFG should include implementation of linear interpolation, lower frame duration to at least one second, and include all list mode data. This would require more time and computer power then what was available in this study.

Different types of gating should be compared, including phase and time based gating, as well as different number of gates. In optimal gating, a smaller efficiency window should be used.

Bibliography

[1] Lori Alma. How does breathing normally work? https://www.verywellhealth.com/physiology-of-breathing-998219, February 2018. Accessed: 14.12.2018.

[2] Abi Berger. How does it work? positron emission tomography. *BMJ (Clinical research ed.)*, 326(7404):1449–1449, 2003.

[3] Ronald Boellaard, Roberto Delgado-Bolton, Wim J. G. Oyen, Francesco Giammarile, Klaus Tatsch, Wolfgang Eschner, Fred J. Verzijlbergen, Sally F. Barrington, Lucy C. Pike, Wolfgang A. Weber, Sigrid Stroobants, Dominique Delbeke, Kevin J. Donohoe, Scott Holbrook, Michael M. Graham, Giorgio Testanera, Otto S. Hoekstra, Josee Zijlstra, Eric Visser, Corneline J. Hoekstra, Jan Pruim, Antoon Willemsen, Bertjan Arends, Jörg Kotzerke, Andreas Bockisch, Thomas Beyer, Arturo Chiti, Bernd J. Krause, and Medicine European Association of Nuclear. Fdg pet/ct: Eanm procedure guidelines for tumour imaging: version 2.0. *European journal of nuclear medicine and molecular imaging*, 42(2):328–354, 2015.

[4] Liu Chi, II Larry, A. Pierce, M. Alessio Adam, and E. Kinahan Paul. The impact of respiratory motion on tumor quantification and delineation in static pet/ct imaging. *Physics in Medicine and Biology*, 54(24):7345, 2009.

[5] Gaspar Delso, Sebastian Fürst, Björn Jakoby, Ralf Ladebeck, Carl Ganter, Stephan G. Nekolla, Markus Schwaiger, and Sibylle I. Ziegler. Performance measurements of the siemens mmr integrated whole-body pet/mr scanner. *Journal of Nuclear Medicine*, 2011.

[6] Sebastian Fürst, Robert Grimm, Inki Hong, Michael Souvatzoglou, Michael E. Casey, Markus Schwaiger, Stephan G. Nekolla, and Sibylle I. Ziegler. Motion correction strategies for integrated pet/mr. 56(2):261–269, 2015.

[7] Partha Ghosh. Improved visualization of small liver metastases using HD•Chest and FlowMotion. https://www.siemens-

healthineers.com/molecular-imaging/case-studies/improved-visualization-of-small-liver-metastases.html, Mar 2014. Accessed: 15.05.19.

[8] Ashley Gillman, Jye Smith, Paul Thomas, Stephen Rose, and Nicholas Dowson. Pet motion correction in context of integrated pet/mr: Current techniques, limitations, and future projections. *Medical Physics*, 44(12):e430–e445, 2017.

[9] Siemens Healthcare GmbH. Syngo MR E11P Operator Manual –MR-PET, 2016. Available upon request from Siemens Healthcare GmbH.

[10] Robert Grimm, Sebastian Fürst, Michael Souvatzoglou, Christoph Forman, Jana Hutter, Isabel Dregely, Sibylle I. Ziegler, Berthold Kiefer, Joachim Hornegger, Kai Tobias Block, and Stephan G. Nekolla. Self-gated mri motion modeling for respiratory motion compensation in integrated pet/mri. *Medical Image Analysis*, 19(1):110–120, 2015.

[11] Robert Grimm, Sebastian Fürst, Isabel Dregely, Stephan G. Nekolla, Sybille Ziegler, Simon Bauer, Dominik Nickel, Berthold Kiefer, Joachim Hornegger, Markus Schwaiger, and T. Block. Mr-pet respiration compensation using self-gated motion modeling. 2012.

[12] I. Hong, S. Fürst, J. Jones, and M. Casey. The strategy of elastic motion corrections. In *2013 IEEE Nuclear Science Symposium and Medical Imaging Conference (2013 NSS/MIC)*, pages 1–5, 2018.

[13] Krzysztof Iniewski. *Medical imaging : principles, detectors, and electronics*. Wiley, Hoboken, N.J., 2009.

[14] Hideo Kaneko and Jun Horie. Breathing movements of the chest and abdominal wall in healthy subjects. *Respiratory Care*, 57(9):1442–1451, 2012.

[15] P. E. Kinahan, D. W. Townsend, T. Beyer, and D. Sashin. Attenuation correction for a combined 3d PET/CT scanner. *Medical Physics*, 25(10):2046–2053, October 1998.

[16] Paul E. Kinahan and James W. Fletcher. Positron emission tomography-computed tomography standardized uptake values in clinical practice and assessing response to therapy. *Seminars in ultrasound, CT, and MR*, 31(6):496–505, 2010.

[17] Zibo Li and Peter S. Conti. Radiopharmaceutical chemistry for positron

emission tomography. *Advanced Drug Delivery Reviews*, 62(11):1031–1051, 2010.

[18] Cancer Registry of Norway. Cancer in Norway 2017 - Cancer incidence, mortality, survival and prevalence in Norway. 2018.

[19] Arifa Pasic, Pieter E. Postmus, and Thomas G. Sutedja. What is early lung cancer?: A review of the literature. *Lung Cancer*, 45(3):267–277, 2004.

[20] V. Schulz, I. Torres-Espallardo, S. Renisch, Z. Hu, N. Ojha, P. Börnert, M. Perkuhn, T. Niendorf, W. M. Schäfer, H. Brockmann, T. Krohn, A. Buhl, R. W. Günther, F. M. Mottaghy, and G. A. Krombach. Automatic, three-segment, mr-based attenuation correction for whole-body pet/mr data. *European Journal of Nuclear Medicine and Molecular Imaging*, 38(1):138–152, 2011.

[21] Bernard W. Stewart. World cancer report 2014. *World Health Organization*, 2014.

[22] Axel Van Der Gucht, Benjamin Serrano, Florent Hugonnet, Benoît Paulmier, Nicolas Garnier, and Marc Faraggi. Impact of a new respiratory amplitude-based gating technique in evaluation of upper abdominal pet lesions. *European Journal of Radiology*, 83(3):509–515, 2014.

[23] Iain Wheatley. Respiratory rate 4: breathing rhythm and chest movement. *Nursing Times*, 114(9):49–50, 2018.

[24] Hugh D. Young and Roger A. Freedman. *Sears and Zemansky's University Physics*, volume One, pages 396–397. Pearson Education Limited, 14. edition, 2016.

[25] S. Ziegler, H. Braun, P. Ritt, C. Hocke, T. Kuwert, and H. H. Quick. Systematic evaluation of phantom fluids for simultaneous PET/MR hybrid imaging. *Journal of Nuclear Medicine*, 54(8):1464–1471, June 2013.

[26] Susanne Ziegler, Bjoern W. Jakoby, Harald Braun, Daniel H. Paulus, and Harald H. Quick. Nema image quality phantom measurements and attenuation correction in integrated pet/mr hybrid imaging. *EJNMMI physics*, 2(1):18–18, 2015.